Preparation of highly dispersible and tumor-accumulative, iron oxide nanoparticles: Multi-point anchoring of PEG-b-poly(4-vinylbenzylphosphonate) improves performance significantly

著者	Ujiie Kodai, Kanayama Naoki, Asai Kei, Kishimoto Mikio, Ohara Yusuke, Akashi Yoshimasa, Yamada Keiichi, Hashimoto Shinji, Oda Tatsuya, Ohkohchi Nobuhiro, Yanagihara Hideto, Kita Eiji, Yamaguchi Masayuki, Fujii Hirofumi, Nagasaki Yukio
journal or publication title	Colloids and surfaces. B, Biointerfaces
volume	88
number	2
page range	771-778
year	2011-12
権利	(C) 2011 Elsevier B.V. “NOTICE: this is the author's version of a work that was accepted for publication in Colloids and surfaces. B, Biointerfaces. Changes resulting from the publishing process, such as peer review, editing, corrections, structural formatting, and other quality control mechanisms may not be reflected in this document. Changes may have been made to this work since it was submitted for publication. A definitive version was subsequently published in Colloids and surfaces. B, Biointerfaces, Volume 88(2), 2011 DOI;10.1016/j.colsurfb.2011.08.013”
URL	http://hdl.handle.net/2241/114739

doi: 10.1016/j.colsurfb.2011.08.013

Preparation of Highly Dispersible and Tumor-Accumulative, Iron Oxide Nanoparticles
-Multi-point Anchoring of PEG-*b*-poly(4-vinylbenzylphosphonate) Improves Performance Significantly-

Kodai Ujiie,[a] Naoki Kanayama,[a] Kei Asai,[a] Mikio Kishimoto,[a] Yusuke Ohara,[b] Yoshimasa Akashi,[b] Keiichi Yamada,[b] Shinji Hashimoto,[b] Tatsuya Oda,[b] Nobuhiro Ohkohchi,[b] Hideto Yanagihara,[a] Eiji Kita,[a] Masayuki Yamaguchi,[c] Hirofumi Fujii,[c] Yukio Nagasaki[a,d,e]*

*Corresponding author. Tel.: (+81)-29-853-5749, Fax.: (+81)-29-853-5749, e-mail address: yukio@nagalabo.jp

a. *Department of Materials Science, Graduate School of Pure and Applied Sciences, University of Tsukuba, 1-1-1 Tennoudai, Tsukuba, Ibaraki 305-8573, Japan*
b. *Department of Surgery, Advanced Biomedical Applications, Graduate School of Comprehensive Human Science, University of Tsukuba, 1-1-1 Tennoudai, Tsukuba 305-8575, Japan*
c. *Function Imaging Division, Research Center for Innovative Oncology National Cancer Center Hospital East, 6-5-1 Kashiwanoha, Kashiwa 277-8577, Japan*
d. *Master's School of Medicinal Sciences, Graduate School of Comprehensive Human Science, University of Tsukuba, 1-1-1 Tennoudai, Tsukuba, Ibaraki 305-8573, Japan*
e. *Satellite Laboratory, International Center for Materials Nanoarchitectonics Satellite (MANA), National Institute for Materials Science (NIMS) and University of Tsukuba, 1-1-1 Tennoudai, Tsukuba, Ibaraki 305-8573, Japan*

Abstract

This paper describes the preparation of iron oxide nanoparticles, surface of which was coated with extremely high immobilization stability and relatively higher density of poly(ethylene glycol) (PEG), which are referred to as PEG protected iron oxide nanoparticles (PEG-PIONs). The PEG-PIONs were obtained through alkali coprecipitation of iron salts in the presence of the PEG-poly(4-vinylbenzylphosphonate) block copolymer (PEG-*b*-PVBP). In this system, PEG-*b*-PVBP served as a surface coating that was bound to the iron oxide surface via multipoint anchoring of the phosphonate groups in the PVBP segment of PEG-*b*-PVBP. The binding of PEG-*b*-PVBP onto the iron oxide nanoparticle surface and the subsequent formation of a PEG brush layer were proved by FT-IR, zeta potential, and thermogravimetric measurements. The surface PEG-chain density of the PEG-PIONs varied depending on the [PEG-*b*-PVBP]/[iron salts] feed-weight ratio in the coprecipitation reaction. PEG-PIONs prepared at an optimal feed-weight ratio in this study showed a high surface PEG-chain surface density (≈ 0.8 chains nm^{-2}) and small hydrodynamic diameter (<50 nm). Furthermore, these PEG-PIONs could be dispersed in phosphate-buffered saline (PBS) that contains 10% serum without any change in their hydrodynamic diameters over a period of one week, indicating that PEG-PIONs would provide high dispersion stability under *in vivo* physiological conditions as well as excellent anti-biofouling properties. In fact we have confirmed the prolong blood circulation time and facilitate tumor accumulation (more than 15 % ID g^{-1} tumor) of PEG-PIONs without the aid of any target ligand in mouse tumor models. The majority of the PEG-PIONs accumulated in the tumor by 96 h after administration, whereas those in normal tissues were smoothly eliminated by 96 h, proving the enhancement of tumor selectivity in the PEG-PION localization. The results obtained here strongly suggest that originally synthesized PEG-*b*-PVBP, having multipoint anchoring character by the phosphonate groups, is rational design for improvement in nanoparticle as *in vivo* application. Two major points, *viz*., extremely stable anchoring character and dense PEG chains tethered on the nanoparticle surface, worked simultaneously to become PEG-PIONs as an ideal biomedical devices intact for prolonged periods in harsh biological environments.

Key Words

PEG / multi-point anchoring / block copolymer / iron oxide nanoparticles / dispersion stability / biodistribution

1. Introduction

A major limitation of nanoparticle-based biodevices for in vivo applications (including drug delivery and imaging) is their nonspecific biodistribution. In general, when the nanoparticles are administered in the bloodstream, they are rapidly bound by plasma components including serum proteins, which results in the formation of aggregates that are rapidly eliminated from the bloodstream because of uptake by reticular endothelial systems (RES) such as macrophages in the liver and spleen [1,2]. Thus, the nanoparticles are nonspecifically accumulated in the liver and spleen before reaching their target site. Several studies have already revealed that the in vivo behavior

of nanoparticles depends greatly on their morphology and surface properties [3-5]. In order to improve the blood circulation behavior as well as the in vivo distribution of nanoparticles, their sizes have to be controlled within the range 10−50 nm. Furthermore, the nanoparticle surface should be engineered to maximally reduce the nonspecific interactions with plasma proteins, since the RES-mediated rapid clearance of nanoparticles is triggered by the adsorption of these proteins on their surfaces.

In this regard, a common approach is the introduction of poly(ethylene glycol) (PEG) chains with an optimal molecular weight onto the nanoparticle surface (so-called "PEGylation"). PEG is a hydrophilic, nonionic, and biocompatible polymer, which stabilizes the nanoparticles in aqueous media mainly through the effects of steric repulsion [6]. Nowadays, PEGylation is regarded as one of the most appropriate methodologies for reducing nonspecific interactions with various biological components and improving the blood circulation of nanoparticles. It has also been recognized that a high PEG-chain density on the surface is essential for the effective suppression of these nonspecific interactions with biological components [7-10]. Thus, despite the prevalence of the PEGylation of nanoparticles, there is a need for further improvement in the surface immobilization density of the PEG chains, as well as in their binding stability to the nanoparticle surface, so that the PEGylated nanoparticles will remain intact in harsh biological environments over long periods.

Previously, we have examined the facile and effective PEGylation of various nanoparticles using PEG-based hydrophilic block copolymers [11-14]. The basic design of our polymeric coatings, which combines the intramolecular microphase separation property and the multipoint anchoring effect, has been proved useful for improving the dispersion stability of various nanoparticles in physiological media. For instance, we demonstrated that the PEG-poly[(2-*N*,*N*-dimethylamino)ethyl methacrylate] block copolymer (PEG-*b*-PAMA) effectively binds to the surface of gold nanoparticles (GNPs) through multipoint coordination of the tertiary amino groups of the PAMA segment [12,13]. The dense and stable PEG brush layer means that the resulting PEGylated GNPs can maintain their dispersed state under harsh conditions (e.g., high salt concentrations, broad pH range) for long periods of time. In addition, the PEGylated GNPs showed high dispersion stability even in the 95% human serum [13]. We also demonstrated the stabilization of Y_2O_3 nanoparticles (YNPs) doped with Er ions using the PEG-poly(acrylic acid) block copolymer (PEG-*b*-PAAc). PEG-*b*-PAAc bound to the YNP surface through multipoint anchoring between the PAAc segment and the YNP surface, resulting in the formation of a PEG brush layer on the surface of the YNP. The dispersion stability of these YNPs in physiological saline was significantly improved by surface treatment with PEG-*b*-PAAc [14].

In this study, we focused our attention on iron oxide nanoparticles (IONs). Over the past two decades, IONs have received a lot of attention because of their high potential for use in various biomedical applications such as MR imaging, drug delivery, and magnetic hyperthermia (including magnetic thermo-ablation)[15-17]. Although there have been large numbers of attempts to PEGylate IONs already [18-32], the improvement of the surface PEG brush density, as well as the PEG brush stability, remains a challenge. Recently, Jeong and Jon et al. reported the application of the poly(3-(trimethoxysilyl)propyl methacrylate)-(poly(ethylene glycol methyl ether methacrylate)) random copolymer for the coating of IONs [29,30]. The trimethoxysilyl groups within this polymer can bind to the ION surface through the formation of

Fe−O−Si bonds or crosslinking with each other under heat treatment. This results in the formation of a robust silica network on the ION surface. A stable PEG brush layer was formed on the ION surface by treatment with this polymer. The resulting IONs formed a stable dispersion under physiological conditions, and after intravenous administration, they accumulated effectively in the tumor without the aid of a targeting ligand. More recently, a novel approach has been developed to obtain highly PEGylated small IONs. This approach is based on the controlled deposition of a thin layer of gold on the ION surface following PEG−SH immobilization through Au−S bond formation [31,32]. However, such methods include complicated and/or multistep procedures for the preparation of PEGylated IONs with adequate stability.

Here, we adopted our surface-coating strategy, which utilizes PEG-based hydrophilic block copolymers to prepare densely and stably PEGylated IONs. In this approach, we employed the PEG-poly(4-vinylbenzylphosphonate) block copolymer (PEG-*b*-PVBP, Scheme 1a). The phosphonate group was chosen because of its well-known ability to bind to various metal oxides including iron oxides [33-38]. The PVBP segment in PEG-*b*-PVBP was anticipated to bind strongly onto the ION surface through multipoint anchoring. In addition, the main-chain structure of the PVBP segment consisting of polystyrene would enhance the anchoring of the PVBP segment onto the ION surface because of its hydrophobic nature, which would prevent the detachment of the surface-bound PEG-*b*-PVBP under harsh biological conditions. IONs covered with PEG-*b*-PVBP (PEG-PIONs) were prepared through the conventional alkali coprecipitation of iron salts in the presence of varying amounts of PEG-*b*-PVBP. Structural and physicochemical characterizations of the PEG-PIONs were carried out using various analytical techniques. The relationship between the surface PEG-chain density and the dispersion stability of the PEG-PIONs under physiological conditions was examined using dynamic light scattering (DLS). Finally, the in vivo distribution of the PEG-PIONs after intravenous administration to tumor-bearing mice was assessed by inductively coupled plasma mass spectrometry (ICP-MS).

2. Materials and methods

2.1. Materials

Materials and synthesis of PEG-*b*-PVBP[39] are described in Supporting Information. The number-averaged molecular weight (*M*n) of PEG segment was 5,000 g mol^{-1}, and the number of repeating units (n) of PVBP segment was 15.

2.2. Measurements

Measurements are described in Supporting Information.

2.3. Preparation of iron oxide nanoparticles covered with PEG-*b*-PVBP (PEG-PIONs)

$FeCl_2 \cdot 4H_2O$ (138 mg, 0.7 mmol) and $FeCl_3 \cdot 6H_2O$ (409 mg, 1.5 mmol) were weighted into a pear-shaped flask and dissolved in 3 mL of water. PEG-*b*-PVBP solution (2 mL in water) was added to this solution and the resulting mixture was stirred for 5 min. NH_4OH (25% v/v in H_2O, 11.3 mL) was added with vigorous stirring. The reaction mixture was allowed to stir at room temperature for 2 h, and then dialyzed (MWCO

20,000) against 2 L of water. The dialysate water was changed after 2, 6, and 12 h, respectively. Unbound (free) PEG-*b*-PVBP was removed by ultrafiltration (PSF membrane, MWCO: 200,000). Four types of PEG-PION were prepared by varying the feed-weight ratio between PEG-*b*-PVBP and iron salts (see Table 1). The resulting PEG-PIONs were dispersed in either deionized water or physiological saline, and were stored at 4 °C before use.

2.4. Cell culture and in vitro cell cytotoxicity assay

C-26 cells were maintained as an adherent culture and grown as a monolayer in a humidified incubator (95% air, 5% CO_2) at 37 °C in a Petri dish containing Dulbecco's modified Eagle's medium (DMEM, Sigma) supplemented with 1% penicillin/streptomycin and 10% heat-inactivated fetal bovine serum (FBS, Gibco). 5×10^3 cells were seeded in each well of a 96-well culture plate and incubated for 24 h. The medium of each well was then replaced with 90 μL of fresh DMEM containing 10% FBS and 10 μL of a PEG-PION dispersion in PBS at selected concentrations. Control experiments were carried out using PBS instead of the PEG-PION dispersion. The culture plate was returned to the incubator and incubated for 24 h. After this incubation period, the medium was removed and the cells were rinsed five times with PBS (pH 7.4). The viability of the cells was evaluated by means of the colorimetric WST assay using Cell Counting Kit-8 (Dojindo, Kumamoto, Japan) according to the manufacturer's instructions. Briefly, 10 μL of WST-8 reagent was added to each well and incubated for 2 h at 37 °C. The absorbance at 450 nm was measured by a Varioscan Flash plate reader (Thermo Fisher Scientific Inc., UK). The results were expressed as a percentage relative to the control.

2.5. In vivo study

All procedures involving animal care were approved by the Animal Ethics Committee of the University of Tsukuba, and were conducted according to the Guidelines for Animal Experimentation of the University of Tsukuba. The blood circulation behavior of PEG-PION4 was examined in normal ICR mice (female; age, 7 weeks; weight, 25-29 g). The PEG-PION4 dispersion in physiological saline was administered intravenously to mice at a dose of 84 mg Fe kg^{-1} mouse, and blood was collected from the heart after defined time periods (0.05, 4, 8, 24, and 48 h). Control experiments were carried out with the intravenous administration of physiological saline instead of the PEG-PION4 dispersion. The Fe concentrations in the collected blood samples were determined by ICP-MS. The in vivo distribution of PEG-PION4 was assessed in C-26 tumor-bearing BALB/c mice 14 days after the implantation of C-26 cells (1×10^6 cells/200 μL per mouse) when the mean tumor volume was >100 mm^3 (female; age, 7 weeks; weight, 23-27 g). The PEG-PION4 dispersion in physiological saline was administered intravenously to the mice at a dose of 84 mg Fe kg^{-1} mouse. Control experiments were carried out with intravenous administration of physiological saline instead of the PEG-PION4 dispersion. For analysis, the mice were sacrificed using the approved method of dislocation of the neck with anesthesia after defined time periods (0.05, 4, 8, 24, 48, and 96 h), after which they were perfused with physiological saline. Major tissues (tumor, heart, lung, kidney, spleen, and liver) were excised and lyophilized. The tissue samples were dissolved in HNO_3/H_2O_2 (3:1 (v/v)) and evaporated to dryness. The residues were redissolved in 0.5 mol L^{-1} HNO_3, and the Fe

content in each tissue sample was determined by ICP-MS measurements.

2.6. In vivo MRI imaging

In vivo MRI imaging was carried out on C-26 tumor-bearing mice. PEG-PIONs were injected intravenously into mice at a dose of 2.1 mg per mouse on the basis of Fe. After 24 h, T_2-weighted FSE imaging was performed. The mice were anesthetized using 1% isoflurane admixed with 50% N_2O and 50% O_2 during imaging.

2.7. Prussian blue staining

The tumor sample excised 24 h after the intravenous administration of PEG-PION4 was fixed in 10% paraformaldehyde, embedded in paraffin, and cut in slices 2 μm in thickness. For Prussian blue staining, the slides were incubated for up to 20 min at room temperature with fresh 2% potassium ferrocyanide in water mixed with an equal volume of 1% hydrochloric acid. Slides were washed, counterstained with nuclear fast red (Kernechtrot stain solution, Muto Pure Chemicals, Japan), and mounted and then photographed with a microscope (BX50F, Olympus Optical Co. Ltd., Tokyo, Japan).

3. Results and discussion

3.1. Preparation of PEG-PIONs

Several methodologies have been established for the preparation of IONs, such as coprecipitation, thermal decomposition, and the hydrothermal method [40]. Among these, coprecipitation of iron salts under alkali conditions is commonly employed, because of its ease of operation and amenable scale-up. In this study, we performed the alkali coprecipitation of iron salts in the presence of PEG-*b*-PVBP to prepare IONs coated with PEG-*b*-PVBP (PEG-PIONs, Scheme 1b). The preparation of metal (oxide) nanoparticles in a liquid phase containing a stabilizer has been shown to be useful for controlling the particle size and the density of the surface-bound stabilizer [12,20,25,41-43]. Aqueous mixtures of iron salts containing various amounts of PEG-*b*-PVBP were prepared, and NH_4OH solution was subsequently added to the mixtures. The color of the solutions changed from yellow to dark red-brown immediately after the addition of NH_4OH, indicating the generation of IONs. After stirring for 2 h at room temperature, the resulting mixture was dialyzed against deionized water to neutralize it and then purified by ultrafiltration until the unbound PEG-*b*-PVBP was completely removed. The removal of the unbound PEG-*b*-PVBP could be monitored by the absorption peak of the filtrate (around 210−250 nm), which corresponds to the benzyl moiety of PEG-*b*-PVBP. During the purification process, no agglomeration was occurred in any of the samples.

3.2. Characterization of PEG-PIONs

The core size of PEG-PIONs was visually confirmed by TEM measurements. For instance, Fig. 1 shows a typical TEM image of PEG-PION1. The number-averaged diameters (d_n) of the PEG-PIONs were determined by TEM image analyses, and the results are summarized in Table 1. In general, the size of IONs generated by the coprecipitation method in the presence of the stabilizer depends on the feed ratio between the stabilizer and the iron salts [41-43]. The core sizes of the PEG-PIONs

prepared in this study, however, were almost identical (≈ 7.7 nm) regardless of the feed ratio of PEG-*b*-PVBP to iron salts. Before the addition of ammonia to the mixture of PEG-*b*-PVBP and iron salt solution, the formation of micelle-like aggregates (hydrodynamic diameter ≈ 30 nm) was observed through DLS measurements. These aggregates presumably act as a "template" leading to the generation of IONs of almost the same size. Powder XRD analyses were performed to confirm the crystalline properties of the PEG-PIONs (data not shown). The obtained results showed characteristic diffraction peaks (2θ = 30.2°, 35.5°, 43.2°, 53.8°, and 57.2°) similar to those of maghemite (γ-Fe_2O_3) and magnetite (Fe_3O_4) [19,25,29,42,43]. The dark red-brown color of the PEG-PION dispersions strongly indicated that the ION core of the PEG-PIONs was mainly in the γ-Fe_2O_3 structure.

To characterize the obtained particles, we carried out FT-IR measurements (Fig. S1 in supporting information). The FT-IR spectra of the PEG-PIONs strongly suggest the existence of PEG-*b*-PVBP on the PEG-PIONs surfaces, showing the characteristic peaks of PEG-*b*-PVBP around 1456 cm^{-1} (ν(C=C)), 1350 cm^{-1} (ν(C=C)), 1247 cm^{-1} (ν(P=O)), 1110 cm^{-1} (ν(P–O)), 946 cm^{-1} (ν(P–O)), and 839 cm^{-1} (δ(C–H)). The existence of PEG-*b*-PVBP on the PEG-PIONs surface was further confirmed by the zeta potential measurements (Fig. 2a). For the bare IONs, the zeta potential varied significantly from highly positive (≈ +35 mV) to negative (≈ -35 mV) with the increasing pH of the medium (from pH 2 to 11). On the contrary, the PEG-PIONs showed a relatively small change in the zeta potential compared to the bare iron oxide particles over the same pH range. In addition, the absolute values of the zeta potentials of the PEG-PIONs were significantly smaller than those of the bare IONs. In particular, the zeta potentials of PEG-PION3 and PEG-PION4 were close to 0 mV regardless of the pH of the medium. These results strongly suggest that the PVBP segment of PEG-*b*-PVBP binds to the iron oxide surface, allowing the formation of a PEG brush layer, as illustrated in Scheme 1b.

The amounts of PEG-*b*-PVBP adsorbed onto the PEG-PION surfaces were examined by TGA. Fig. S2 in supporting information shows the TGA thermograms of free PEG-*b*-PVBP and PEG-PIONs. The free PEG-*b*-PVBP revealed characteristic two-step thermal decomposition behavior (Fig. S2a). The distinct weight losses observed around 370−400 °C and 460−520 °C correspond to the thermal decomposition of the PEG segment and polystyrene moiety, respectively. Accordingly, the resulting mass observed at over 550 °C (ca. 28%) can be regarded as corresponding to the phosphonate moieties. For the PEG-PIONs, the degree of weight loss increased with an increase in the [PEG-*b*-PVBP]/[iron salts] feed ratio (Fig. S2b−e). The surface PEG-chain density on each PEG-PION sample was estimated from the percentage weight loss at 650 °C (WL_{650}) and d_n of each ION core (Table 1), under the following assumptions: (i) the mass remaining at over 550 °C corresponds to the fraction of ION core and P_2O_5 (the major product of organic phosphonates by thermal decomposition [44]); (ii) the density of the ION core is 4.89 $g \cdot cm^{-3}$ (as γ-Fe_2O_3) [45]; and (iii) all PEG-*b*-PVBP chains are anchored onto the ION core surface as a single layer. As depicted in Fig. 2b, the surface PEG-chain density on the PEG-PIONs gradually increased with an increase in the [PEG-*b*-PVBP]/[iron salts] feed ratio, and reached a plateau above [PEG-*b*-PVBP]/[iron salts] = 0.35. This is consistent with the results of the zeta potential measurements of PEG-PIONs. The maximum surface PEG-chain density on the PEG-PIONs prepared here was ≈ 0.8 chains$\cdot nm^{-2}$, which is significantly higher than found for previous

PEGylated IONs (below 0.4 chains·nm^{-2}) [20,22,25-30].

3.3. Dispersion stability of PEG-PIONs

As mentioned in the Introduction, the dispersion stability of the IONs under physiological conditions is crucial for their systemic administration. The dispersion stability of PEG-PIONs in PBS was assessed by DLS. For PEG-PION1 and PEG-PION2, the particles flocculated just after their dispersion in PBS, and obvious precipitation was observed within 1 h (data not shown). On the contrary, PEG-PION3 and PEG-PION4 dispersed stably into PBS and showed no significant changes in their hydrodynamic diameters over a period of more than two weeks (Fig. 3a). These results indicate that the surface PEG-chain density greatly influences the dispersion stability of PEG-PIONs, as reported previously [13]. Phosphate salts from PBS are known to bind to the metal oxide surface and/or displace with the chemisorbed stabilizer, resulting in a decrease in the dispersion stability [37,47]. Riffle et al. reported that the hydrodynamic diameter of IONs covered with monophosphonate-functionalized PEG gradually increased in PBS over 24 h [37]. More recently, we showed that the monophosphonate-functionalized PEG adsorbed onto an Y_2O_3 surface easily displaced with phosphate salts in PBS [40]. Both PEG-PION3 and PEG-PION4 could maintain their dispersion in PBS without any change in their hydrodynamic diameters over a period of two weeks. This long-term dispersion stability in the presence of phosphate salts is presumably due to the multipoint anchoring of the PVBP segment of PEG-*b*-PVBP onto the ION core surface. Such multipoint anchoring of the PVBP segment might make it difficult for the PEG-*b*-PVBP to be replaced by the phosphate salts in PBS. In addition, the hydrophobic nature of the polystyrene backbone of the PVBP segment might enhance the stability of the PEG brush layer on the ION surface.

The excellent dispersion stabilities of PEG-PION3 and PEG-PION4 were also confirmed in the serum-containing medium. These samples formed stable dispersions in 10% FBS containing PBS without any change in their hydrodynamic diameters for over one week (Fig. 3b). It should be noted that the hydrodynamic diameters of PEG-PION3 and PEG-PION4 were almost identical to those in the absence of FBS (Fig. 3a). This strongly suggests that both PEG-PION3 and PEG-PION4 possess excellent anti-biofouling surface properties.

3.4. Cytotoxicity of PEG-PIONs

To assess the potential toxicity of PEG-PION3 and PEG-PION4, a WST assay was performed using C-26 cells. The results shown in Fig. S3 (in Supporting Information) indicate that both PEG-PION3 and PEG-PION4 have little effect on cell viability even at high concentrations. The amount of Fe at the highest concentration was ≈ 30 mg Fe mL^{-1} which was higher than that of typical ION-based MR imaging agents for mice (1−15 mg Fe mL^{-1}). Thus, we concluded that PEG-PION3 and PEG-PION4 have minimal toxicity.

3.5. Biodistribution of PEG-PIONs

In the previous section, we revealed that PEG-PION3 and PEG-PION4 possess an excellent anti-biofouling properties and high dispersion stabilities under physiological conditions. It is also noteworthy that PEG-PION4 maintained its hydrodynamic size below 50 nm for over one week, even in the presence of serum proteins. This retention

of a consistent particle size is important from the viewpoint of improving blood circulation behavior, since larger nanoparticle sizes facilitate phagolytic clearance [3-5]. From the results obtained, we anticipated that PEG-PION4 could circumvent recognition by RES and prolong blood circulation.

The blood circulation behavior of PEG-PION4 in mice was assessed by following the variation in the Fe content in the blood after intravenous administration (84 mg Fe kg^{-1} of dose). The results are expressed as the mean percentage of injected dose (% ID) mL^{-1} blood, and are plotted against post-injection time (Fig. 4a). As anticipated, PEG-PION4 showed stable circulation in the bloodstream; 24 h after intravenous administration, 14.1 % ID mL^{-1} of PEG-PION4 remained in the blood. In contrast, the commercial Ferucarbotran (Resovist) showed a very short blood circulation time (< 5 % ID mL^{-1} blood 3 h after intravenous administration) under the same administration conditions, presumably because of rapid clearance by RES.

The accumulation behavior of PEG-PION4 in the major organs (heart, lung, kidney, spleen, liver, and tumor) after intravenous administration to tumor-bearing mice was assessed by ICP-MS (Fig. 4b). Interestingly, although PEG-PION4 has no tumor-targeting ligand molecules the ICP-MS results revealed continuous accumulation of PEG-PION4 in the tumor after intravenous administration. More than 15 % ID g^{-1} tumor of PEG-PION4 accumulation was confirmed from 8 h after intravenous administration, and this could be detected by in vivo MR imaging. The T_2-weighted image at 24 h after intravenous administration showed that the MR signal intensity of the tumor decreased significantly, allowing clear identification of the tumor (Fig. 5, tumor site indicated by the arrow). To our knowledge, there have been only a few reports on the effective accumulation of polymer-coated IONs (more than 15 % ID g^{-1} tumor) through systemic administration without the aid of any targeting ligand [29,30,32]. The distribution of PEG-PION4 in the tumor tissue was visualized by Prussian blue staining. As shown in Fig. 6, PEG-PION4 was distributed around the tumor blood vessels to the outside through the leaky from the tumor vascular walls (indicated by the arrow), suggesting that PEG-PION4 accumulated in the tumor tissue through the enhanced permeability and retention (EPR) effect [47]. The small hydrodynamic size, neutral surface charge, and excellent anti-biofouling surface properties of PEG-PION4 should make its EPR-effect-mediated tumor-specific accumulation feasible.

Significant accumulation of PEG-PION4 in normal tissues such as the liver and spleen was also confirmed by ICP-MS analyses. Its accumulation in the liver peaked at 24 h after injection (15.8 % ID g^{-1} tissue). However, it is interesting to note that the accumulated PEG-PION4 then started to be washed out, as was confirmed by ICP-MS. Eventually, the accumulated level of PEG-PION4 in the liver was reduced to 4.8 % ID g^{-1} tissue at 96 h after injection. A similar accumulation/clearance tendency was also confirmed in other normal tissues including the spleen. On the contrary, for the tumor tissue, the accumulated PEG-PION4 showed only a moderate clearance, and 13.4 % ID g^{-1} tissue of PEG-PION4 still remained even at 96 h after injection. This is presumably due to the defective and/or suppressed lymphatic drainage in the tumor [47]. The metabolic difference in PEG-PION4 between normal and tumor tissues observed here is useful not only for enhancing its selective localization in tumor tissue, but also for promoting the safety of its administration, since long-term accumulation of inorganic nanoparticles in the living body often causes unexpected injury [48-50]. Although the

detailed mechanism is not clear at this stage, we believe that the favorable metabolic properties of PEG-PION4 are closely related to the size and surface properties of these nanoparticles.

4. Conclusions

In this study, we have demonstrated the preparation of PEGylated IONs (PEG-PIONs) by the simple coprecipitation reaction of iron salts in the presence of PEG-*b*-PVBP. In our approach, PEG-*b*-PVBP served as a surface coating and was robustly anchored to the ION surface via multipoint chemical bond formation between the ION surface and the phosphonate groups in the PVBP segment of PEG-*b*-PVBP. PEG-PIONs prepared under optimal conditions (PEG-PION4) showed a sufficiently high surface PEG-chain density (≈ 0.8 chains·nm^{-2}) and small hydrodynamic diameter (< 50 nm). Furthermore, PEG-PION4 could be dispersed in 10% serum containing PBS without any change in its hydrodynamic diameter over a period of one week, indicating its high dispersion stability under physiological conditions, as well as its excellent anti-biofouling properties. These features of PEG-PION4 prolonged its blood circulation time and facilitated its EPR-effect-mediated tumor accumulation after intravenous administration to tumor-bearing mice. The majority of the PEG-PION4 accumulated in normal tissues (such as the liver and spleen) was smoothly eliminated up to 96 h after administration, whereas most of the PEG-PION4 accumulated in the tumor remained there even at 96 h after administration, and 13.4 % ID g^{-1} tumor of PEG-PION4 was detected by ICP-MS analysis. This metabolic difference in PEG-PION4 between normal and tumor tissues is thought to enhance the selectivity of its localization in tumor tissue. Our approach would be beneficial for developing tumor-targeted and safe ION-based biomedical devices. Finally, we wish to emphasize that the molecular design of PEG-*b*-PVBP is rational for the construction of PEGylated-ION-based biomedical devices that remain intact under harsh biological condition over long periods of time, and also that PEG-*b*-PVBP can be applied for the effective surface PEGylation of other nanoparticles such as metal oxides and ceramics.

Acknowledgements

This work was supported by a Grant-in-Aid for Scientific Research on Innovative Areas, “Molecular Soft-Interface Science” (No.20106011), and the World Premier International Research Center (WPI) Initiative on Materials Nanoarchitectonics (MANA) of the Ministry of Education, Culture, Sports, Science and Technology (MEXT) of Japan.

References

[1] S. M. Moghimi, A. C. Hunte, J. C. Murray, Pharmacol. Rev. 53 (2001) 283-318.
[2] D. E. Owens, N. A. Peppas, Int. J. Pharm. 307 (2006) 93-102.
[3] R. Weissleder, A. Bogdanov, E. A. Neuwel, M. Papisov, Adv. Drug Delivery Rev. 16 (1995) 321-334.
[4] A. K. Gupta, M. Gupta, Biomaterials 26 (2005) 3995-4021.
[5] J. Huang, L. Bu, J. Xie, K. Chen, Z. Cheng, X. Li, X. Chen, ACS Nano 4 (2010) 7151-7160.
[6] J. M. Harris ed., "Poly(Ethylene Glycol)Chemistry: Biotechnical and Biomedical Applications", Plenum Press, New York (1992).
[7] M. Malmsten, K. Emoto, J. M. Van Alstine, J. Colloid Interface Sci. 202 (1998) 507-517.
[8] S. Pasche, J. Volrols, H. J. Griesser, N. D. Spencer, M. Textor, J. Phys. Chem. B 109 (2005) 17545-17552.
[9] L. D. Unsworth, H. Sheardown, J. L. Brash, Langmuir, 21 (2005) 1036-1041.
[10] K. Uchida, H. Otsuka, M. Kaneko, K. Kataoka, Y. Nagasaki, Anal. Chem. 77 (2005) 1075-1080.
[11] Y. Nagasaki, Chem. Lett. 37 (2008) 564-569.
[12] T. Ishii, H. Otsuka, K. Kataoka, Y. Nagasaki, Langmuir 20 (2003) 561-564.
[13] D. Miyamoto, M.Oishi, K. Kojima, K. Yoshimoto, Y. Nagasaki, Langmuir 24 (2008) 5010-5017.
[14] M. Kamimura, D. Miyamoto, Y. Saito, K. Soga, Y. Nagasaki, Langmuir 24 (2008) 8864-8870.
[15] P. Majewski, B. Thierny, Crit. Rev. Solid State Mater. Sci. 32 (2007) 203-215.
[16] R. Hao, R. Xing, Z. Xu, Y. Hou, S. Gao, S. Sun, Adv. Mater. 22 (2010) 2729-2742.
[17] O. Veiseh, J. W. Gunn, M. Zhang, Adv. Drug Delivery Rev. 62 (2010) 284-304.
[18] L. X. Tiefenauer, A. Tschirky, G. Kühne, R. Y. Andres, Magn. Reson. Imaging 14 (1996) 391-402.
[19] L. A. Harris, J. D. Goff, A. Y. Carmichael, J. S. Riffle, J. J. Harburn, T. G. St. Pierre, M. Saunders, Chem. Mater. 15 (2003) 1367-1377.
[20] J.-F. Lutz, S. Stiller, A. Hoth, L. Kaufner, U. Pison, R. Cartier, Biomacromolecules 7 (2006) 3132-3138.
[21] M. Kumagai, Y. Imai, T. Nakamura, Y. Yamasaki, M. Sekino, S. Ueno, K. Hanaoka, K. Kikuchi, T. Nagano, E. Kaneko, K. Shimokado, K. Kataoka, Colloids Surf. B 56 (2007) 174-181.
[22] M. Kumagai, M. R. Kano, Y. Morishita, M. Ota, Y. Imai, N. Nishiyama, M. Sekino, S. Ueno, K. Miyazono, K. Kataoka, J. Controlled Rel. 140 (2009) 306-311.
[23] T. K. Jain, M. K. Reddy, M. A. Morales, D. L. L.-Pelecky, V. Labhasetwar, Mol. Pharm. 5 (2008) 316-327.
[24] F. Hu, K. W. MacRenaris, E. A. Waters, T. Liang, E. A. S.-Sikma, A. L. Eckermann, T. J. Meade, J. Phys. Chem. C 113 (2009) 20855-20860.
[25] P. Papaphilippou, L. Loizou, N. C. Popa, A. Han, L. Vekas, A. Odysseos, T. K.-Christoforou, Biomacromolecules 10 (2009) 2662-2671.
[26] S. Liu, B. Jia, R. Qiao, Z. Yang, Z. Yu, Z. Liu, K. Liu, J. Shi, H. Ouyang, F. Wang, M. Gao, Mol. Pharm. 6 (2009) 1074-1082.

[27] K.Chen, J. Xie, H. Xu, D. Behera, M. H. Michalski, S. Biswal, A. Wang, X. Chen, Biomaterials 30 (2009) 6912-6919.
[28] H. Chen, L. Wang, J. Yeh, X. Wu, Z. Cao, Y. A. Wang, M. Zhang, L. Yang, H. Mao, Biomaterials 31 (2010) 5397-5407.
[29] H. Lee, E. Lee, D. K. Kim, N. K. Jang, Y. Y. Jeong, S. Jon, J. Am. Chem. Soc. 128 (2006) 7383-7389.
[30] H. Lee, M. K. Yu, S. Park, S. Moon, J. J. Min, Y. Y. Jeong, H-.W. Kang, S. Jon, J. Am. Chem. Soc. 129 (2007) 12739-12745.
[31] H. Kojima, Y. Mukai, M. Yoshikawa, K. Kamei, T. Yoshikawa, M. Morita, T. Inubushi, T. A. Yamamoto, Y. Yoshioka, N. Okada, S. Seino, S. Nakagawa, Bioconj. Chem. 21 (2010) 1026-1031.
[32] M. Kumagai, T. K. Sarma, H. Cabral, S. Kaida, M. Sekino, N. Herlambang, K. Osada, M. R. Kano, N. Nishiyama, K. Kataoka, Macromol. Rapid Commun. 31 (2010) 1521-1528.
[33] V. Zoulalian, S. Monge, S. Zürcher, M. Textor, J. J. Robin, S. Tosatti, J. Phys. Chem. B 110 (2006) 25603-25605.
[34] C. A. Traina, J. Schwartz, Langmuir 23 (2007) 9158-9161.
[35] L. Qi, A. Sehgal, J.-C. Castaing, J.-P. Chapel, J. Fresnais, J.-F. Barret, F. Cousin, ACS NANO 2 (2008) 879-888.
[36] G. Guerrero, P. H. Mutin, A. Vioux, Chem. Mater. 13 (2001) 4367-4373.
[37] J. D. Goff, P. P. Huffstetler, W. C. Miles, N. Pothayee, C. M. Reinholz, S. Ball, R. M. Davis, J. S. Riffle, Chem. Mater. 21 (2009) 4784-4795.
[38] U. I. Tromsdorf, O. T. Bruns, S. C. Salmen, U. Beisiegel, H. Weller, Nano Lett. 9 (2009) 4434-4440.
[39] M. Kamimura, N. Kanayama, K. Tokuzen, K. Soga, Y. Nagasaki, Nanoscale, in press (DOI: 10.1039/c1nr10466g).
[40] S. Laurent, D. Forge, M. Port, A. Roch, C. Robic, L. V. Elst, R. N. Muller, Chem. Rev. 108 (2008) 2064-2110.
[41] F. Jones, H. Colfen, M. Antonietti, Colloid Polym. Sci. 278 (2000) 491-501.
[42] S. Si, A. Kotal, T. K. Mandal, S. Giri, H. Nakamura, T. Kohara, Chem. Mater. 16 (2004) 3489-3496.
[43] L. Gu, Z. Shen, C. Feng, Y. Li, G. Lu, X. Huang, G. Wang, J. Huang, J. Mater. Chem. 18 (2008) 4332-4340.
[44] Lj. Tušek-Božič, R. Trojko, J. Therm. Anal. Cal. 81 (2005) 153-157.
[45] A. F. Thünemann, J. Kegel, J. Polte, F. Emmerling, Anal. Chem. 80 (2008) 5905-5911.
[46] W. C. Miles, J. D. Goff, P. P. Huffstetler, C. M. Reinholz, N. Pothayee, B. L. Caba, J. S. Boyd, R. M. Davis, J. S. Riffle, Langmuir 25 (2009) 803-813.
[47] Y. Matsumura, H. Maeda, Cancer Res. 46 (1986) 6387-6392.
[48] H. S. Choi, W. Liu, P. Misra, E. Tanaka, J. P. Zimmer, B. I. Ipe, M. G. Bawendi, J. V. Frangioni, Nat. Biotech. 25 (2007) 1165-1170.
[49] V. I. Shubayev, T. R. Pisanic II, S. Jin, Adv. Drug Deliv. Rev., 61 (2009) 467-477.
[50] M. A. Voinov, J. O. S. Pagán, E. Morrison, T. I. Smirnova, A. I Sminov, J. Am. Chem. Soc. 133 (2011) 35-41.

FIGURE CAPTIONS

Fig. 1 TEM image of PEG-PION1. Inset is size distribution of PEG-PION1 obtained by TEM analysis.

Fig. 2 **a)** Zeta potential vs. pH plot for bare IONs (solid square), PEG-PION1 (open triangle), PEG-PION2 (solid triangle), PEG-PION3 (open circle), and PEG-PION4 (solid circle). Data expressed are means of triplicate measurements (± S.D.). **b)** Change in the surface PEG chain density on PEG-PIONs with (PEG-*b*-PVBP)/(iron salts) feed ratio.

Fig. 3 Hydrodynamic diameters of PEG-PION3 (open circle) and PEG-PION4 (solid circle) upon incubation in (a) PBS, (b) 10 % of FBS containing PBS at room temperature.

Fig. 4 **a)** Blood circulation behavior of PEG-PION4 (open circle), commercial ferucarbotran (solid circle) after intravenous administration to ICR mice (Dose: 84 mg Fe kg^{-1} mouse, N= 5). The levels of Fe in blood are shown as the mean percentage of injected dose (% ID) mL^{-1} blood at each time period. **b)** Biodistribution of PEG-PION4 after intravenous administration to C-26 tumor bearing mice (Dose: 84 mg Fe kg^{-1} mouse, N = 5). The levels of Fe in tumor (open circle), liver (solid circle), spleen (open triangle), kidney (solid triangle), lung (open square) and heart (solid square) are shown as the mean percentage of injected dose (% ID) g^{-1} tissue at each time period.

Fig. 5 T_2-weightened images of C-26 tumor bearing mice at 24 h post-injection of 84 mg Fe kg^{-1} of PEG-PION4 (a) and control (b). The arrow denotes tumor site.

Fig. 6 Photograph of C-26 xenograft tumor tissue stained by Prussian blue. The blue area indicates the existence of PEG-PION4.

Scheme 1 (a) Chemical structure of PEG-*b*-PVBP. (b) Schematic illustration of suspected structure of PEG-PIONs prepared in this study.

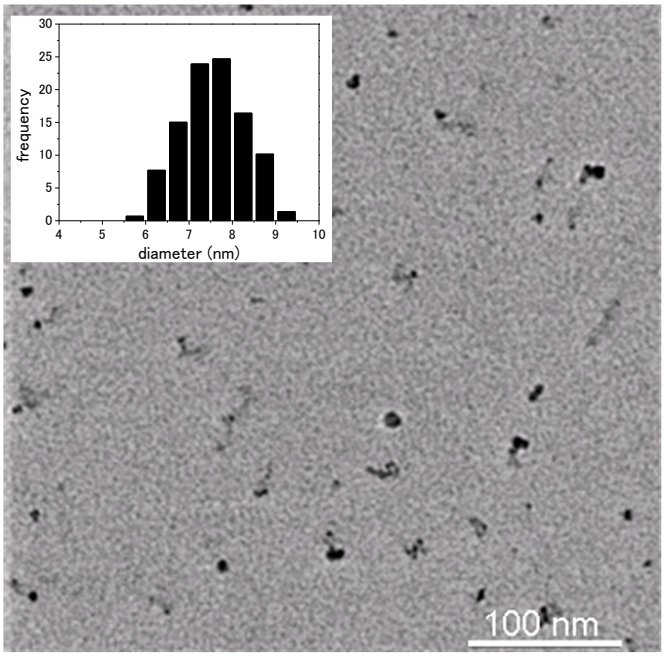

Figure 1

Ujiie et al.

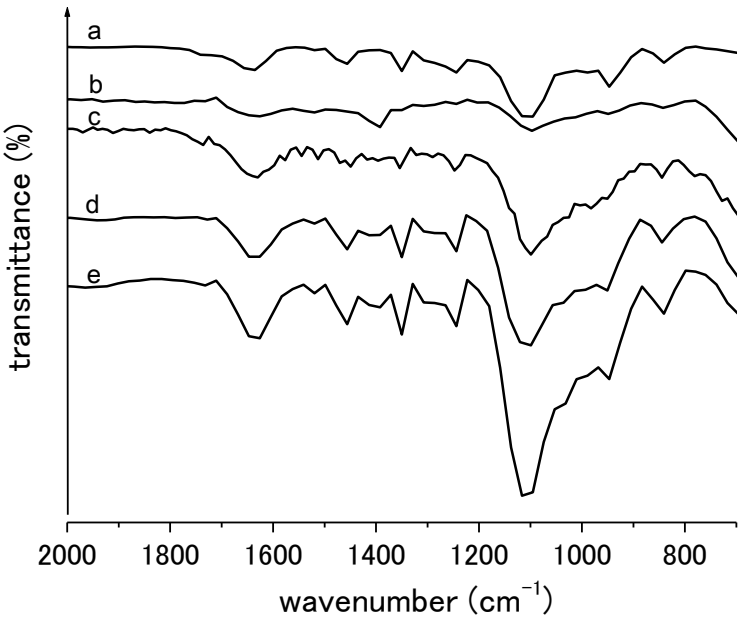

Figure 2

Ujiie et al.

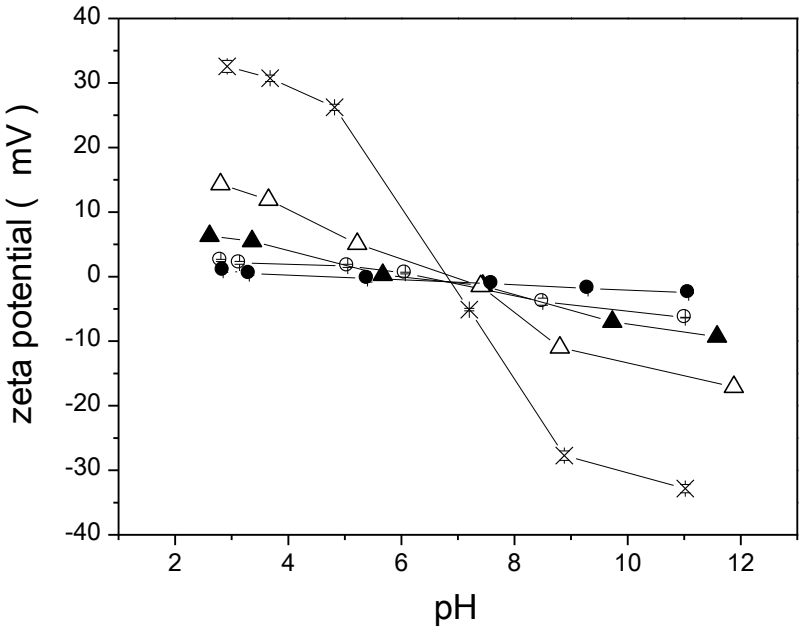

Figure 3

Ujiie et al.

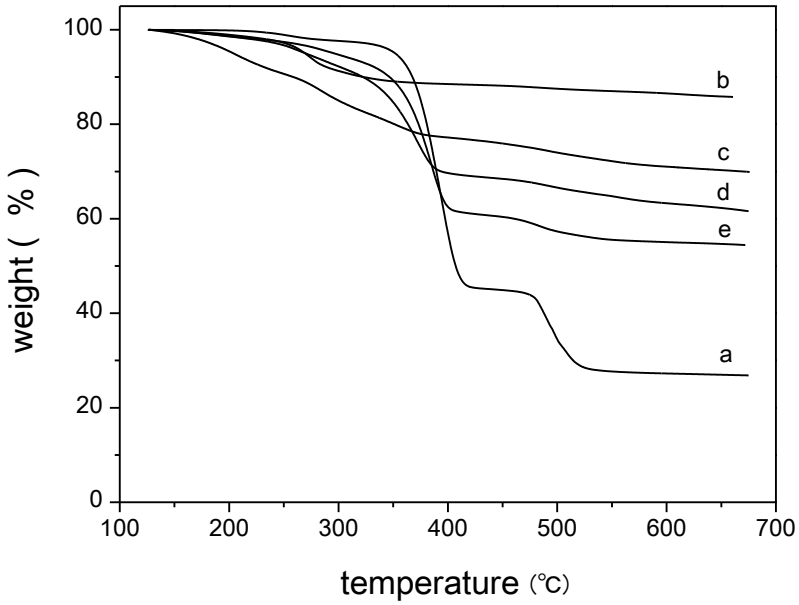

Figure 4

Ujiie et al.

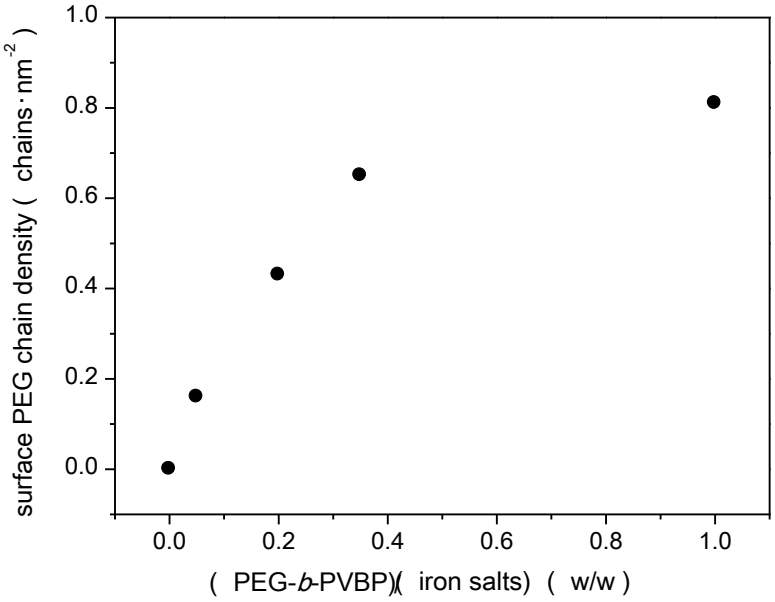

Figure 5

Ujiie et al.

(a)

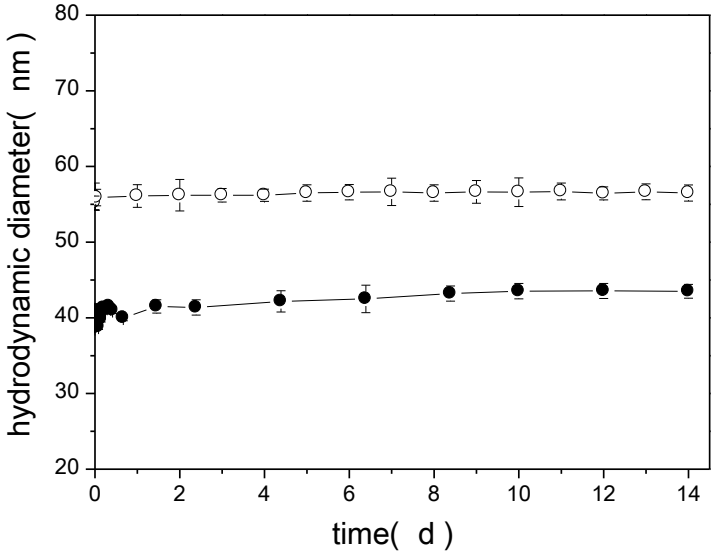

(b)

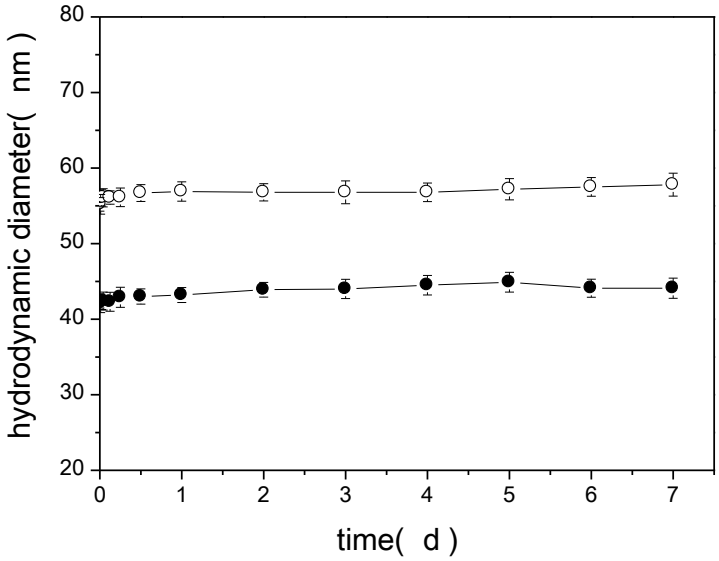

Figure 6

Ujiie et al.

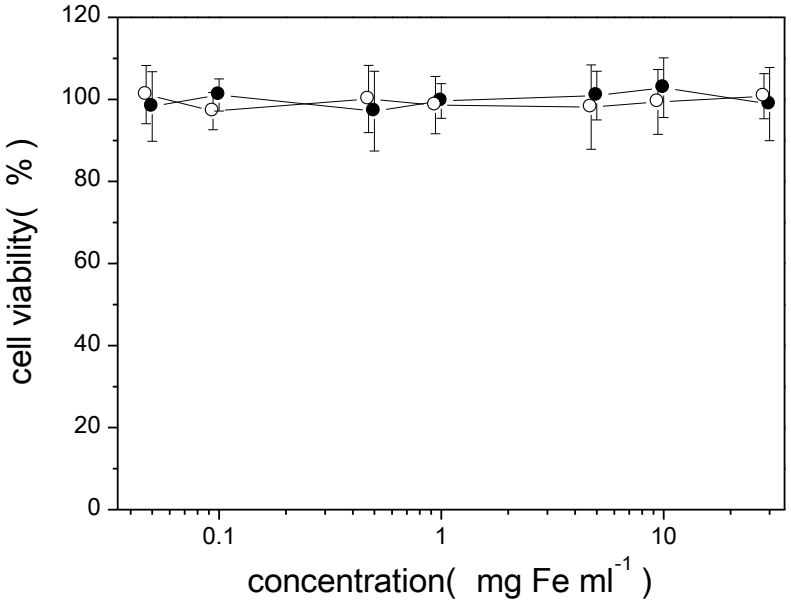

Figure 7

Ujiie et al.

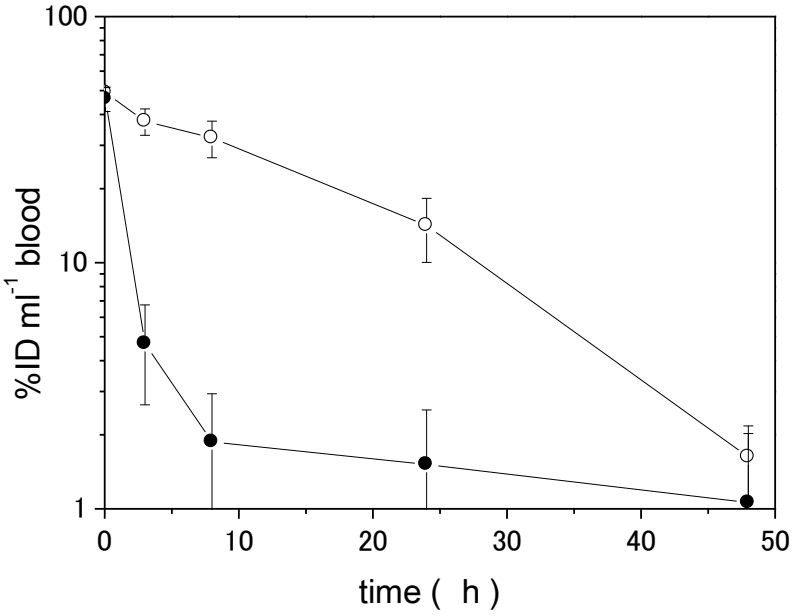

Figure 8

Ujiie et al.

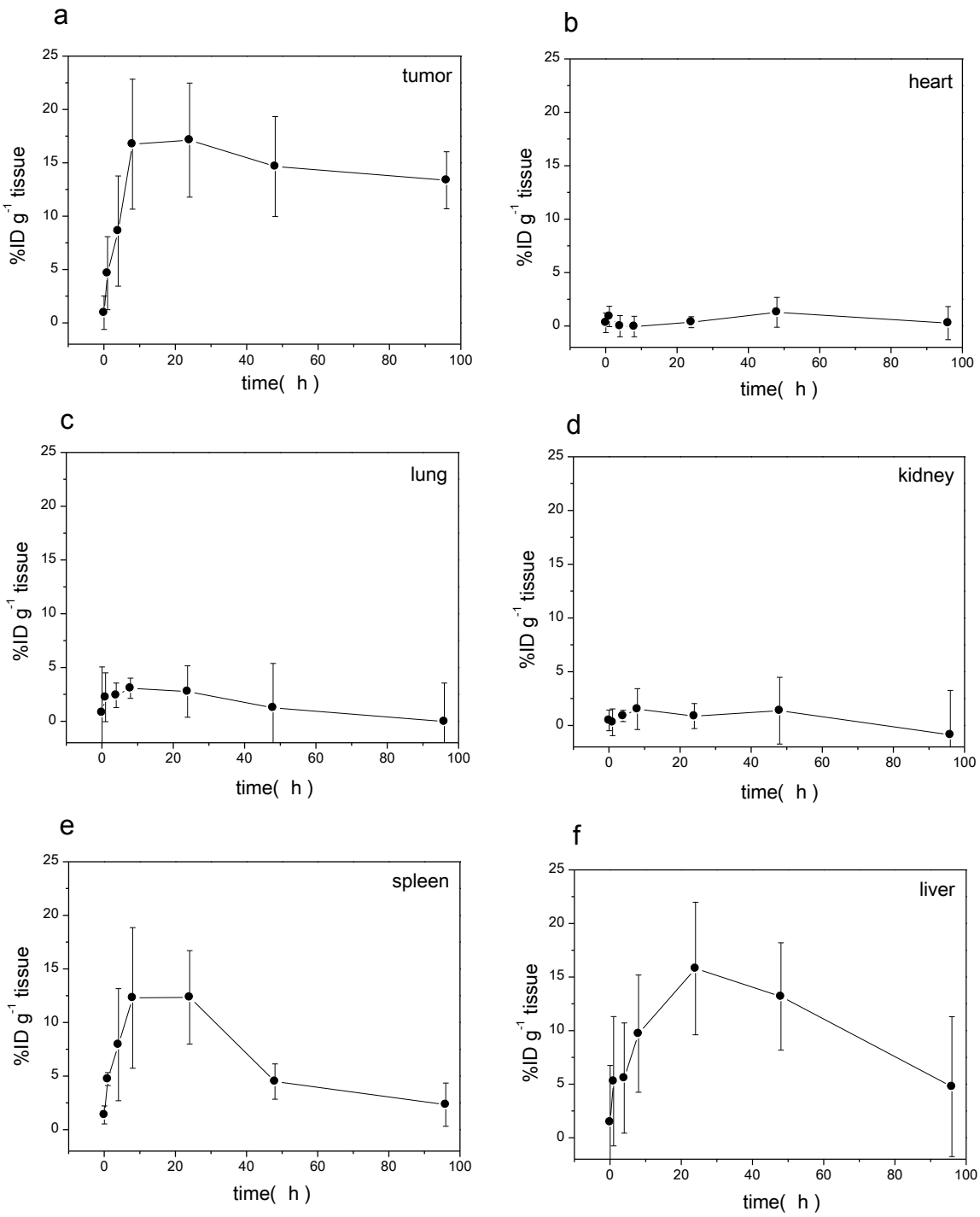

Figure 9

Ujiie et al.

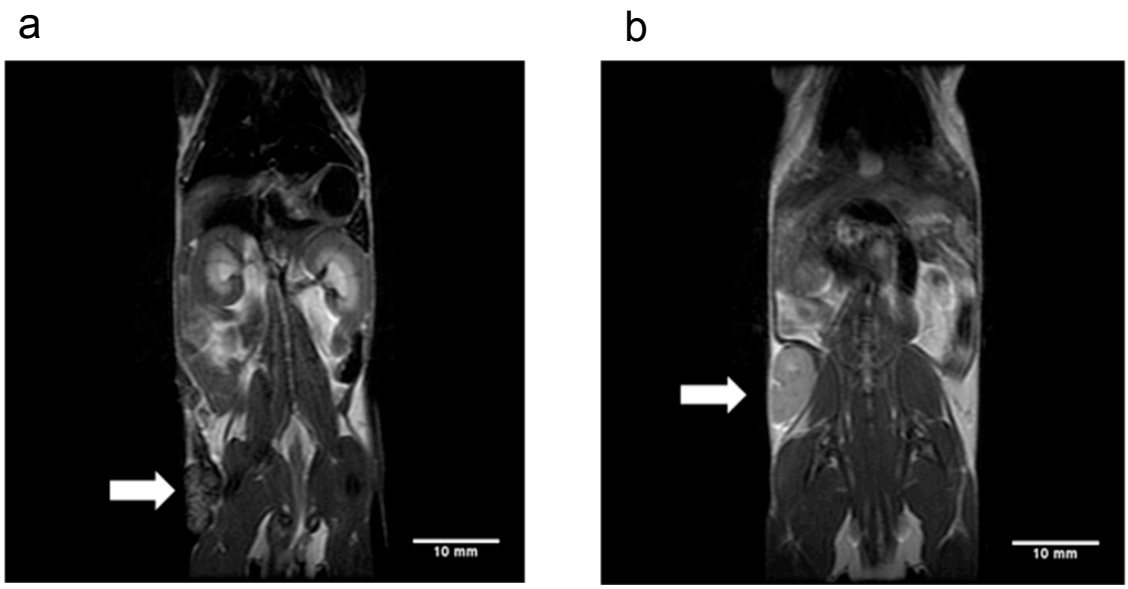

Figure 10

Ujiie et al.

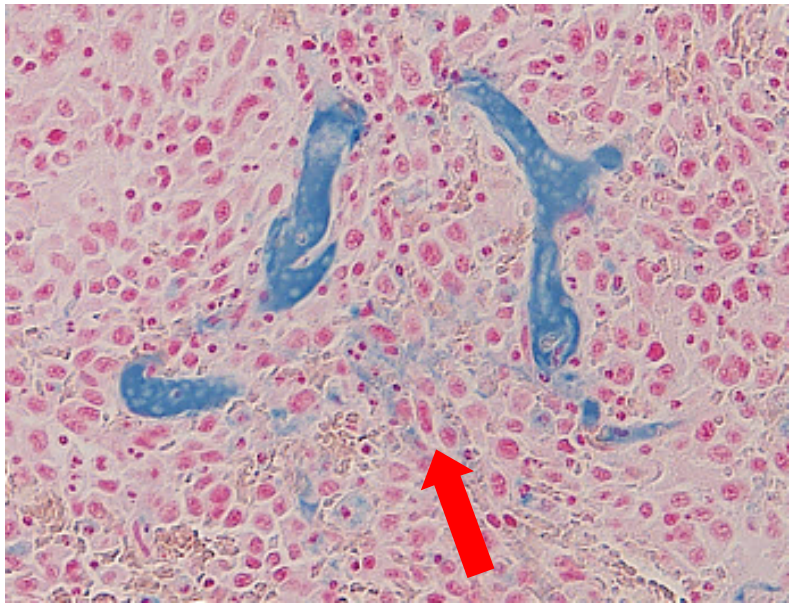

Figure 11

Ujiie et al.

a

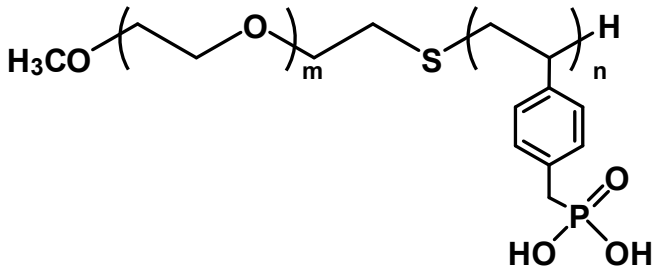

b

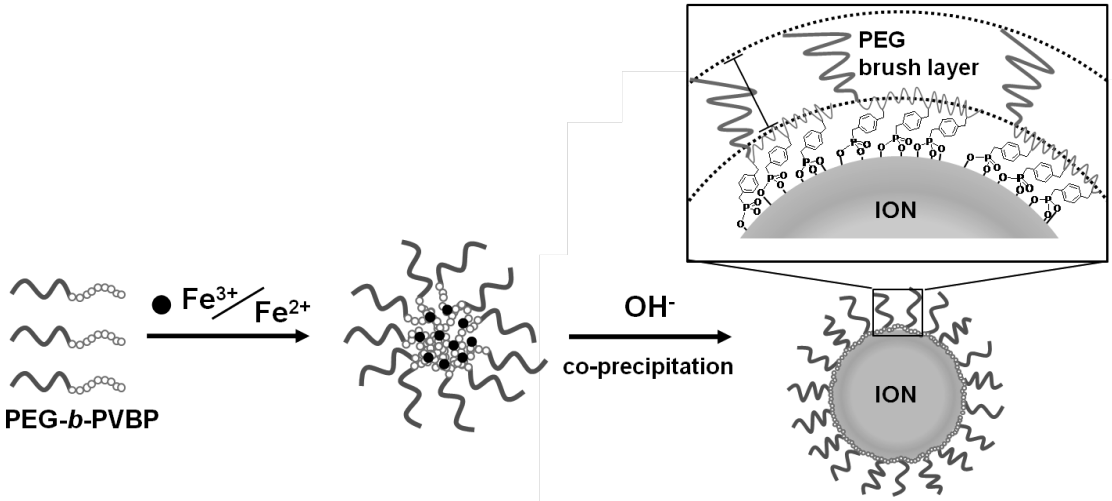

Scheme 1

Ujiie et al.

Supplementary Material

Preparation of Highly Dispersible and Tumor-Accumulative, Iron Oxide Nanoparticles
-Multi-point Anchoring of PEG-*b*-poly(4-vinylbenzylphosphonate) Improves Performance Significantly-

Kodai Ujiie,[a] Naoki Kanayama,[a] Kei Asai,[a] Mikio Kishimoto,[a] Yusuke Ohara,[b] Yoshimasa Akashi,[b] Keiichi Yamada,[b] Shinji Hashimoto,[b] Tatsuya Oda,[b] Nobuhiro Ohkohchi,[b] Hideto Yanagihara,[a] Eiji Kita,[a] Masayuki Yamaguchi,[c] Hirofumi Fujii,[c] Yukio Nagasaki[a,d,e]*

*Corresponding author. Tel.: (+81)-29-853-5749, Fax.: (+81)-29-853-5749, e-mail address: yukio@nagalabo.jp

a. *Department of Materials Sceiences, Graduate School of Pure and Applied Sciences, University of Tsukuba, 1-1-1 Tennoudai, Tsukuba, Ibaraki 305-8573, Japan*
b. *Department of Surgery, Advanced Biomedical Applications, Graduate School of Comprehensive Human Science, University of Tsukuba, 1-1-1 Tennoudai, Tsukuba 305-8575, Japan*
c. *Function Imaging Division, Research Center for Innovative Oncology National Cancer Center Hospital East, 6-5-1 Kashiwanoha, Kashiwa 277-8577, Japan*
d. *Master's School of Medicinal Sciences, Graduate School of Comprehensive Human Science, University of Tsukuba, 1-1-1 Tennoudai, Tsukuba, Ibaraki 305-8573, Japan*
e. *Satellite Laboratory, International Center for Materials Nanoarchitectonics Satellite (MANA), National Institute for Materials Science (NIMS) and University of Tsukuba, 1-1-1 Tennoudai, Tsukuba, Ibaraki 305-8573, Japan*

<Contents>

S-1. Materials

All reagents were commercially available and were used as received. PEG-*b*-PVBP was synthesized by the two-step side-chain conversion of the PEG-poly (4-chloromethylstyrene) block copolymer, which was prepared by our previous method [S1]. The quantitative conversion of the chloromethyl side chains into phosphonic acid groups was confirmed by both ^{1}H- and ^{31}P-NMR spectroscopy. The number-averaged molecular weight (M_n) of the PEG segment was 5,000 g mol^{-1}, and the degree of polymerization of the PVBP segment (n) was 15. Details of the synthesis of PEG-*b*-PVBP are reported elsewhere [S2]. Murine colon adenocarcinoma 26 (C-26) cells were obtained from RIKEN BioResource Center. ICR mice (female; age, 7 weeks; weight, 25−29 g) and BALB/c mice (female; age, 5 weeks; weight, 17−22 g) were purchased from Charles River Japan Inc. Deionized water (>18.1 MΩ cm) purified with a Milli-Q instrument (Millipore, Billerica, MA) was used for all of the experiments.

S-2. Measurements

UV-Vis measurements were conducted on a UV2400 PC spectrophotometer (Shimadzu, Kyoto, Japan), and FT-IR measurements on an FT/IR-300 spectrometer (JASCO, Tokyo, Japan). FT-IR spectra were collected by the KBr pellet method at a resolution of 4 cm^{-1} with 128 scans. DLS and zeta potential measurements were carried out using a Zetasizer Nano ZS (Malvern Instruments, Ltd., U.K.) equipped with a 10-mW He-Ne laser (λ = 633 nm), which produces vertically polarized incident beams at a detection angle of 173°. Thermogravimetric analysis (TGA) was performed using an SII EXTRA6000 DSC/TG/DTA thermal analyzer (Seiko Instrument Inc., Chiba, Japan). Lyophilized samples were first held at 140 °C for 20 min to eliminate moisture, and then the temperature was ramped at a rate of 10 °C min^{-1} to a maximum of 900 °C. All TGA experiments were performed under an Ar flow (200 mL min^{-1}) to minimize sample oxidation. TEM images were obtained using a HITACHI H-800 transmission electron microscope (Hitachi Ltd., Tokyo, Japan) at an accelerating voltage of 80 kV. For TEM sample preparation, ION dispersions were diluted and deposited on a carbon-coated copper grid and allowed to air-dry. The obtained images were analyzed using Image J software (NIH). Powder X-ray diffraction measurements were performed on an RINT-2200 X-ray diffractometer (RIGAKU, Tokyo, Japan) with CuK_α radiation. ICP-MS measurements were performed on an ELAN DRC-e ICP-MS spectrometer (Perkin-Elmer Sciex, UK). In vivo MRI images were obtained using a 3-T Signa HDx whole-body MRI scanner (GE Healthcare, Milwaukee, WI). A body coil was used to transmit radiofrequency (RF) pulses, and a 3-turn solenoid coil dedicated for animal experiments was used to receive the signal. For the T_2-weighted fast spin-echo (FSE) images of living mice, the following parameters were applied: repetition time (TR) = 4000 ms, echo time (TE) = 69 ms, flip angle (FA) = 90°, number of excitations (NEX) = 2. The images were obtained with a field of view (FOV) of 6 × 3 cm, a 256 × 160 matrix, and a 1-mm slice thickness (THK).

S-3. Characterization of PEG-PION

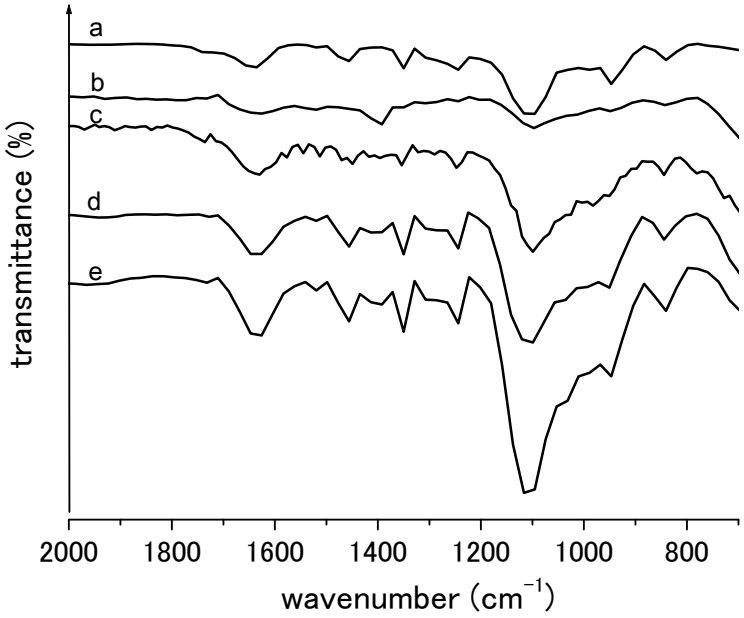

Fig. S1 FT-IR spectra of (a) PEG-b-PVBP, (b) PEG-PION1, (c) PEG-PION2, (d) PEG-PION3, and (e) PEG-PION4.

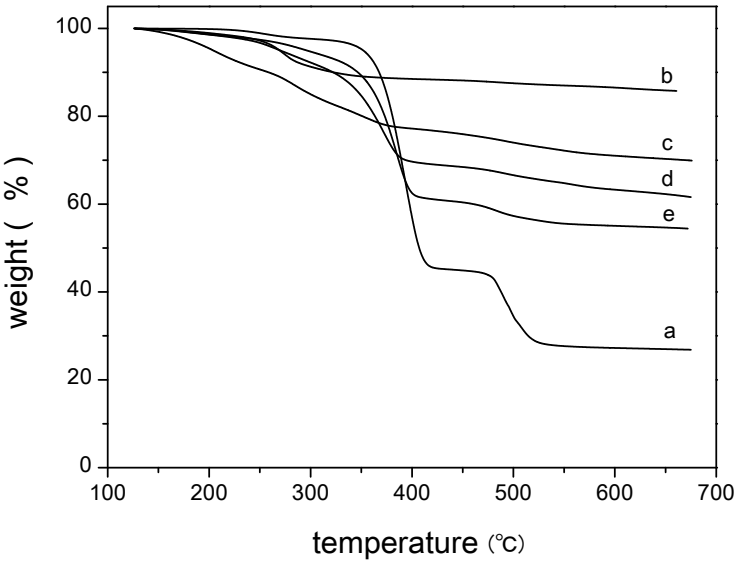

Fig. S2 TG thermograms of (a) PEG-b-PVBP, (b) PEG-PION1, (c) PEG-PION2, (d) PEG-PION3, and (e) PEG-PION4.

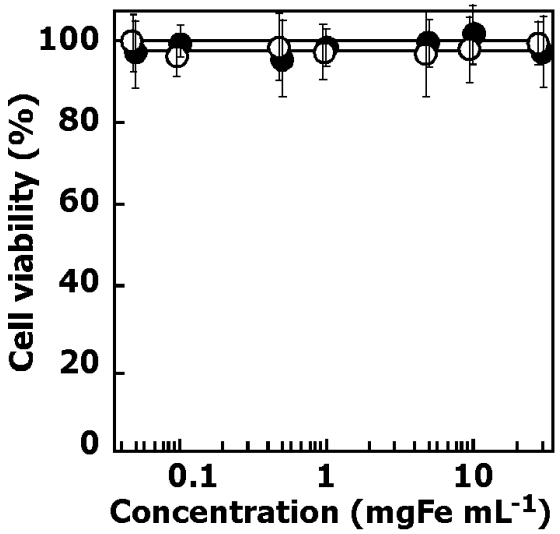

Fig. S3 Viability of C-26 cells after the 24-h incubation with PEG-PION3 (open circle) and PEG-PION4 (solid circle) at various concentrations.

S-4. Reaferences

[S1] T. Yoshitomi, D. Miyamoto, Y. Nagasaki, Biomacromolecules 10 (2010) 596-601.

[S2] M. Kamimura, N. Kanayama, K. Tokuzen, K. Soga, Y. Nagasaki, Nanoscale, in press (DOI: 10.1039/c1nr10466g).